


**Dynamically stabilized spin superfluidity in frustrated magnets**Ricardo Zarzuela <sup>1</sup>, Daniel Hill,<sup>2</sup> Jairo Sinova,<sup>1,3</sup> and Yaroslav Tserkovnyak<sup>2</sup><sup>1</sup>*Institut für Physik, Johannes Gutenberg Universität Mainz, D-55099 Mainz, Germany*<sup>2</sup>*Department of Physics and Astronomy, University of California, Los Angeles, California 90095, USA*<sup>3</sup>*Institute of Physics Academy of Sciences of the Czech Republic, Cukrovarnická 10, 162 00 Praha 6, Czech Republic*

(Received 7 December 2020; revised 28 April 2021; accepted 30 April 2021; published 20 May 2021)

We study the onset of spin superfluidity, namely, coherent spin transport mediated by a topological spin texture, in frustrated exchange-dominated magnetic systems, engendered by an external magnetic field. We show that for typical device geometries used in nonlocal magnetotransport experiments, the magnetic field stabilizes a spin superflow against fluctuations up to a critical current. For a given current, the critical field depends on the precessional frequency of the texture, which can be separately controlled. We contrast such dynamic stabilization of a spin superfluid to the conventional approaches based on topological stabilization.

DOI: [10.1103/PhysRevB.103.174424](https://doi.org/10.1103/PhysRevB.103.174424)**I. INTRODUCTION**

Collective low-dissipation spin transport raises a range of interesting basic questions, while offering promising perspectives for efficient spintronic devices [1,2]. A prominent example lies in the concept of spin superfluidity [3–7], introduced in the late '70s by analogy with the phenomena of (charge) superconductivity and mass superfluidity in <sup>4</sup>He, albeit not exempt from dissipation associated with order-parameter dynamics. One of the hallmarks of spin superfluidity is the algebraic decay of spin signals over long distances, in contrast to the exponential suppression observed for (incoherent) magnon-mediated transport [8–10]. Experimental signatures of superfluid spin transport have been recently reported in (high-quality) antiferromagnetic platforms for device geometries usually used in nonlocal magnetotransport measurements [11,12]. However, parasitic anisotropies arising naturally in the fabrication process of spintronic (collinear) magnetic systems have a detrimental effect on the spin superfluid state, since these break the underlying spin O(2) symmetry of the (anti)ferromagnetic host and, therefore, open a gap in the excitation spectrum that lifts the Goldstone mode sustaining the spin superflow.

Magnetic systems with frustrated interactions dominated by isotropic exchange offer an alternative route to overcome these key challenges by averaging the parasitic anisotropies out at the macroscopic level and restoring an effective SO(3) symmetry in the spin space. Furthermore, the minimal description of these noncollinear magnetic platforms is provided by the O(4)-nonlinear sigma model [13–15], whose excitation spectrum for bulk systems consists of three Goldstone branches. An external magnetic field affects two of these soft (angular) modes, gapping out one of them and distorting the other (the dispersion relation is almost quadratic in the long wavelength limit) [16]. The remaining linearly dispersing mode (corresponding to rotations along the direction of the magnetic field), in turn, is able to sustain a

phase-coherent precessional state, which can be triggered by (interfacial) spin-orbit torques [17]. In particular, for the nonlocal device geometries usually considered (i.e., thin films with an out-of-plane orientation of the spin accumulations and the external magnetic field), the collective flapping out of the basal plane initiates the unwinding (phase slips) of the order parameter. Therefore, disturbing these angular modes by an external magnetic field could impede the (topological) relaxation channel for the spin superflow, enhancing its stability.

We remark that the robustness of a conventional superfluid or superconductor is based on the metastability of a winding order-parameter texture, which derives from its topological character. A static winding texture of a SO(3)-valued order parameter, however, lacks such a topological protection, due to its ability to smoothly unravel the winding angle in multiples of  $4\pi$  [17]. It is, thus, vital to understand to what extent the fluctuations of the SO(3)-valued order parameter are detrimental to a collective spin flow in frustrated magnets. In this paper, we discuss how the stability of a spin-carrying winding texture is restored dynamically, in the presence of collective precession around an applied magnetic field. More specifically, we show that the in-plane (rotational) Goldstone mode can sustain spin supercurrents and study the corresponding steady-state solution. We also examine the robustness of the underlying phase-coherent spin configuration against collective fluctuations and determine its stability threshold as a function of the magnetic field and the precessional frequency. In this regard, we show that even though, under purely topological considerations, there is a low-energy route for the collective relaxation of the spin-superfluid state, the analysis of its dynamics dictates a finite range of stable solutions. It is, therefore, not topology, which is dictated by the free energy (as, e.g., in the case of easy-plane anisotropies [17]), that is key here but a field-induced dynamic stabilization of the basal winding textures.

## II. EQUATIONS OF MOTION

At the macroscopic level, frustrated magnets are described by a SO(3) order parameter,  $\hat{R}(\vec{r}, t)$ , which represents smooth and slowly varying rotations of the initial spin configuration [13,18]. Dynamics of  $\hat{R}$  and the nonequilibrium spin density  $\mathbf{m}(\vec{r}, t)$  of the system are governed by the equations [16,17]

$$\mathbf{m} = \chi(\boldsymbol{\omega} + \gamma\mathbf{B}), \quad (1)$$

$$\partial_t \mathbf{m} + \alpha s \boldsymbol{\omega} = \mathcal{A} \vec{\nabla} \cdot \vec{\Omega} + \gamma \mathbf{m} \times \mathbf{B}, \quad (2)$$

where  $\chi$ ,  $\gamma$ , and  $\mathcal{A}$  denote the spin susceptibility, the gyromagnetic ratio, and the order-parameter stiffness, respectively. Furthermore,  $\alpha$  parametrizes losses due to dissipative processes (Gilbert damping) in the bulk and  $s \simeq \hbar S/a^3$ , with  $S$  and  $a$  being the length of the microscopic spin operators and the lattice spacing, respectively.  $\mathbf{B}$  denotes the external magnetic field,  $\boldsymbol{\omega} \equiv i\text{Tr}[\hat{R}^\dagger \hat{L} \partial_t \hat{R}]/2$  is the local precessional frequency, and the spin fields  $\Omega_k \equiv i\text{Tr}[\hat{R}^\dagger \hat{L} \partial_k \hat{R}]/2$ ,  $k = x, y, z$  describe the spatial variations of the instantaneous state of the spin texture, with  $[\hat{L}_\alpha]_{\beta\gamma} \equiv -i\epsilon_{\alpha\beta\gamma}$  being the generators of the SO(3) group. We note that the dissipative term  $\alpha s \boldsymbol{\omega}$  in Eq. (2) is the one responsible for the algebraic decay of the spin signal when balanced with the appropriate boundary conditions for the spin supercurrent, as we will show in the next section.

By incorporating Eq. (1) into Eq. (2), we obtain the dynamical equation

$$\partial_t \boldsymbol{\omega} = v_m^2 \vec{\nabla} \cdot \vec{\Omega} + \gamma(\boldsymbol{\omega} \times \mathbf{B} - \partial_t \mathbf{B}) - \frac{1}{T} \boldsymbol{\omega}, \quad (3)$$

where  $v_m \equiv \sqrt{\mathcal{A}/\chi}$  denotes the speed of spin waves in the magnetic medium and  $T \equiv \chi/\alpha s$  defines a characteristic relaxation time. A convenient representation of the order parameter is given in terms of unit-norm quaternions,  $\mathbf{q} = (w, \mathbf{v})$  [17], which exhibit a group structure endowed by the Hamilton product  $\mathbf{q}_1 \wedge \mathbf{q}_2 \equiv (w_1 w_2 - \mathbf{v}_1 \cdot \mathbf{v}_2, w_1 \mathbf{v}_2 + w_2 \mathbf{v}_1 + \mathbf{v}_1 \times \mathbf{v}_2)$  and the adjoint operation  $\mathbf{q}^* \equiv (w, -\mathbf{v})$ . In this regard, we note that the parametrization  $w = \cos(\phi/2)$  and  $\mathbf{v} = \sin(\phi/2)\mathbf{n}$ , where  $\mathbf{n}$  and  $\phi(\vec{r}, t)$  represent the rotation axis and the local rotation angle for spins, respectively, yields the well-known Rodrigues' rotation formula:  $\hat{R}_{\alpha\beta} = \cos\phi \delta_{\alpha\beta} + (1 - \cos\phi)n_\alpha n_\beta + \sin\phi \epsilon_{\alpha\gamma\beta} n_\gamma$ . In the quaternion representation, the identities  $\boldsymbol{\omega} = 2\partial_t \mathbf{q} \wedge \mathbf{q}^*$  and  $\Omega_k = 2\partial_k \mathbf{q} \wedge \mathbf{q}^*$ ,  $k = x, y, z$ , hold, so by applying the Hamilton product  $\mathbf{q}^* \wedge \cdot$  with the adjoint to Eq. (3), we obtain the following equation of motion for the order parameter (see Appendix A):

$$\begin{aligned} \partial_t^2 \mathbf{q} + \frac{1}{T} \partial_t \mathbf{q} - v_m^2 \vec{\nabla}^2 \mathbf{q} + \lambda(\mathbf{q})\mathbf{q} \\ - \gamma \left( \mathbf{B}^* \wedge \partial_t \mathbf{q} + \frac{1}{2} \partial_t \mathbf{B}^* \wedge \mathbf{q} \right) = 0, \end{aligned} \quad (4)$$

where  $\lambda(\mathbf{q}) \equiv \partial_t \mathbf{q} \odot \partial_t \mathbf{q}^* - v_m^2 \partial_k \mathbf{q} \odot \partial_k \mathbf{q}^* + \frac{\gamma}{2} \boldsymbol{\omega} \cdot \mathbf{B}$  is a quadratic prefactor,  $\mathbf{B} \equiv (0, \mathbf{B})$ , and the scalar product reads  $\mathbf{q}_1 \odot \mathbf{q}_2 \equiv \frac{1}{2}(\mathbf{q}_1 \wedge \mathbf{q}_2^* + \mathbf{q}_2 \wedge \mathbf{q}_1^*) = w_1 w_2 + \mathbf{v}_1 \cdot \mathbf{v}_2$ .

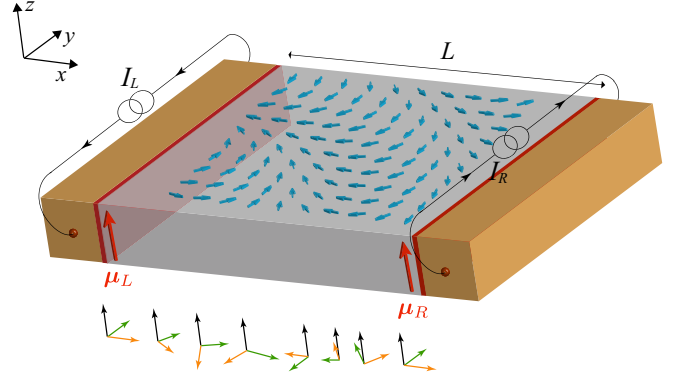


FIG. 1. Two-terminal geometry for the generation and detection of spin superfluidity in frustrated magnetic platforms. The spin precession (blue arrows) along the spin accumulations  $\mu_{L,R}$  (red arrows) is depicted as a rotating triad of vectors, which represents the internal spin frame of the texture. The black arrow represents the rotation axis  $\mathbf{n}$  and the local rotation angle  $\phi$  is illustrated by the rotation of the green and orange arrows of each triad within the plane perpendicular to  $\mathbf{n}$  (which is oriented along the  $z$  axis here).

## III. SPIN SUPERFLUID STATE

Hereafter, we restrict ourselves to a quasi-one-dimensional geometry by assuming translational symmetry along the  $y$  and  $z$  spatial directions, and a finite length  $L$  along the  $x$  direction, see Fig. 1. We also consider lateral contacts extending along the  $yz$  plane for spin injection via spin Hall physics [19] and assume that the spin accumulations  $\mu_L$  (left interface) and  $\mu_R$  (right interface) are parallel to the  $z$  axis, which set the (uniform) direction of  $\mathbf{n} = \hat{e}_z$  across the sample. Furthermore, we apply the magnetic field collinear as well,  $\mathbf{B} = B\mathbf{n}$ , to stabilize the superflow, and take  $\phi(\vec{r}, t)$  to be spatially smooth and slowly varying. As a result, Eq. (4) turns into the following dynamical equation for the rotation angle (see Appendix B):

$$\partial_t^2 \phi + \frac{1}{T} \partial_t \phi - v_m^2 \partial_x^2 \phi + \gamma \partial_t B = 0. \quad (5)$$

The precessional steady solution to the above equation is obtained by considering the ansatz  $\phi(x, t) = X(x) + \tau(t)$ . This separation of variables yields, for a uniform external magnetic field, the system of equations

$$\tau''(t) + \frac{1}{T} \tau'(t) + \gamma \partial_t B = \mu, \quad X''(x) = \frac{\mu}{v_m^2}, \quad (6)$$

with  $\mu$  being a constant to be determined. The solutions to these ordinary differential equations read

$$\tau(t) = \tau_0 + \mu T t - \gamma e^{-t/T} \int_{-\infty}^t B(t') e^{t'/T} dt', \quad (7)$$

$$X(x) = X_0 + kx + \frac{1}{2} \frac{\mu}{v_m^2} x^2, \quad (8)$$

with  $X_0$ ,  $\tau_0$ , and  $k$  being constants to be determined by imposing boundary conditions. The latter are given by

$$-2\mathcal{A} \partial_x \mathbf{q} \wedge \mathbf{q}^*|_L = \frac{g_L}{4\pi} [\mu_L - 2\hbar \partial_t \mathbf{q} \wedge \mathbf{q}^*|_L], \quad (9)$$

$$2\mathcal{A} \partial_x \mathbf{q} \wedge \mathbf{q}^*|_R = \frac{g_R}{4\pi} [\mu_R - 2\hbar \partial_t \mathbf{q} \wedge \mathbf{q}^*|_R], \quad (10)$$

which arise from the exchange of angular momentum between the magnet and adjacent (heavy-)metal contacts in the form of ordinary exchange torques and enhanced Gilbert damping [16,17]. Here,  $g_L$  and  $g_R$  denote the spin mixing conductance at the left ( $x = -\frac{L}{2}$ ) and right ( $x = \frac{L}{2}$ ) terminals, respectively [20]. In what follows, we assume the same spin mixing conductance at both interfaces,  $g \equiv g_L = g_R$ . By considering the solution Eqs. (7) and (8) for the phase-coherent precessional state and a static magnetic field, the above boundary conditions turn into the following linear system of equations for  $k$  and  $\mu$  (see Appendix B):

$$\mathcal{A} \left[ k + \frac{\mu}{v_m^2} \left( -\frac{L}{2} \right) \right] = \frac{g_L}{4\pi} [-\mu_L + \hbar\mu T], \quad (11)$$

$$\mathcal{A} \left[ k + \frac{\mu}{v_m^2} \left( \frac{L}{2} \right) \right] = \frac{g_R}{4\pi} [\mu_R - \hbar\mu T]. \quad (12)$$

We can therefore conclude that the spin superfluid state is described, under an external static magnetic field, by

$$\phi_s(x, t) = \phi_0 + kx + \frac{1}{2} \left( \frac{\alpha S}{\mathcal{A}} \right) \omega x^2 + \omega t, \quad (13)$$

with

$$k = \frac{g}{8\pi\mathcal{A}} (\mu_R - \mu_L), \quad (14)$$

$$\omega = \frac{g}{2} \frac{\mu_L + \mu_R}{\hbar g + 2\pi\alpha S L}. \quad (15)$$

We note in passing that the external magnetic field has no effect on the spin texture sustaining the spin superflow, since we have found the same steady-state solutions as in Refs. [8,9].

#### IV. FLUCTUATIONS AND STABILITY

We proceed next to study the robustness of the spin superfluid state, Eq. (13), against fluctuations of the order parameter. First, we introduce the following orthonormal set  $\{\mathbf{q}_s, \xi_1, \xi_2, \xi_3\}$  of quaternions, where  $\mathbf{q}_s$  corresponds to the superfluid solution given by Eq. (13),  $\xi_1 = (0, \hat{e}_y)$ ,  $\xi_2 = (0, \hat{e}_x)$ , and  $\xi_3 = 2\partial_{\phi_s} \mathbf{q}_s = (-\sin(\phi_s/2), \cos(\phi_s/2)\hat{e}_z)$ . Note that  $\xi_{1,2}$  represent  $\pi$  rotations around the  $y$  and  $x$  axes, respectively. We incorporate fluctuations into the order parameter via the following parametrization:

$$\mathbf{q} = \mathbf{q}_s \sqrt{1 - 2|\Psi_t|^2 - \Psi_l^2} + \hat{e}_+ \Psi_t + \hat{e}_- \Psi_t^* + \xi_3 \Psi_l, \quad (16)$$

where  $\Psi_t$  (complex valued) and  $\Psi_l$  (real valued) represent the transverse and longitudinal (with respect to the rotation axis) fluctuation modes of the (unit-norm) quaternion order parameter. Here,  $\hat{e}_{\pm} \equiv \frac{1}{\sqrt{2}}(\xi_1 \pm i\xi_2)$  are chiral quaternions with the properties  $\hat{e}_{\pm}^2 = 0$  and  $\hat{e}_+ \odot \hat{e}_- = \hat{e}_- \odot \hat{e}_+ = 1$ . We note that the transverse fluctuation modes  $\Psi_t$  correspond to the out-of-plane rotations along the  $x$  and  $y$  axes, which become hybridized by the magnetic field. By inserting this parametrization into Eq. (4) and keeping terms up to first order in  $\Psi_t$  and  $\Psi_l$ , we obtain the following dynamical equations for

the fluctuation fields:

$$\partial_t^2 \Psi_l + \frac{1}{T} \partial_t \Psi_l - v_m^2 \partial_x^2 \Psi_l = 0, \quad (17)$$

$$\begin{aligned} \partial_t^2 \Psi_t + \left( \frac{1}{T} - i\gamma B \right) \partial_t \Psi_t - v_m^2 \partial_x^2 \Psi_t \\ + \frac{1}{4} [(\partial_t \phi_s)^2 - v_m^2 (\partial_x \phi_s)^2 + 2\gamma B \partial_t \phi_s] \Psi_t = 0. \end{aligned} \quad (18)$$

Stability analysis of Eq. (17) in Fourier space (with respect to the  $x$  coordinate) yields the eigenvalues

$$\lambda_t^{\pm}(q) = \frac{1}{2T} \left[ \pm \sqrt{1 - \frac{q^2}{q_c^2}} - 1 \right], \quad (19)$$

where  $q$  and  $q_c \equiv 1/2v_m T$  denote the Fourier wave vector and its critical value, respectively. For  $|q| \leq q_c$ , the eigenvalues of the dynamical system are real valued and negative,  $\lambda_t^{\pm} \leq 0$ . For  $|q| > q_c$  the eigenvalues are complex valued,  $\lambda_t^{\pm}(q) = -\frac{1}{2T} \pm i\Omega(q)$ . Consequently,  $\bar{\Psi}_l \propto e^{\lambda_t^{\pm} t} \sim e^{-t/2T}$  decays exponentially with time, so the spin superfluid solution Eq. (13) is robust against longitudinal fluctuations. This is in agreement with the fact that rotations within the basal ( $xy$ ) plane cannot unwind the order parameter.

In the case of transverse fluctuations, we suppose that the winding of the superfluid phase, described by  $\partial_x \phi_s$ , changes smoothly across the magnet. As a result, we perform a local stability analysis of the  $\Psi_t$  modes supposing  $\partial_x \phi_s \simeq k$  is approximately constant. Again, by Fourier transforming Eq. (18), we obtain the dynamical system

$$\begin{aligned} \partial_t^2 \bar{\Psi}_t + \left( \frac{1}{T} - i\gamma B \right) \partial_t \bar{\Psi}_t \\ + \left[ \frac{\omega^2}{4} + v_m^2 \left( q^2 - \frac{k^2}{4} \right) + \frac{\gamma}{2} \omega B \right] \bar{\Psi}_t = 0, \end{aligned} \quad (20)$$

where  $\bar{\psi}(q, t) \equiv \mathcal{F}[\psi(x, t)]$  denotes the Fourier transform of the fluctuation field. Stability analysis of the above dynamical system yields the eigenvalues

$$\lambda_t^{\pm} = \frac{1}{2} \left\{ -\frac{1}{T} \pm \text{Re}(Z) + i[\gamma B \pm \text{Im}(Z)] \right\}, \quad (21)$$

with  $Z \equiv \sqrt{(i\gamma B - \frac{1}{T})^2 - (\omega^2 + v_m^2(4q^2 - k^2) + 2\gamma\omega B)}$ . Transverse fluctuations proliferate (i.e., their amplitude blows up as time increases) if the exponent  $-\frac{1}{T} \pm \text{Re}(Z)$  is positive. Since  $\text{Re}(Z) = r^{1/2} \cos(\theta/2)$ , with  $re^{i\theta} \equiv Z^2 = [\frac{1}{T^2} + v_m^2 k^2 - (\omega + \gamma B)^2 - 4v_m^2 q^2] - i[\frac{2\gamma B}{T}]$ , we can describe the instability region via the inequality

$$r + r \cos \theta \geq \frac{2}{T^2}, \quad (22)$$

which, after some algebra, yields the relation  $v_m^2 k^2 \geq \omega^2 + 4v_m^2 q^2 + 2\gamma\omega B$ , assuming a finite  $T$ . The highest magnetic field satisfying the latter inequality occurs for  $q = 0$ , from which we derive the following critical value for the magnetic field, above which the phase-coherent precessional state Eq. (13) is robust against fluctuations of the order parameter:

$$2\gamma B_c = \frac{v_m^2 k^2}{\omega} - \omega. \quad (23)$$

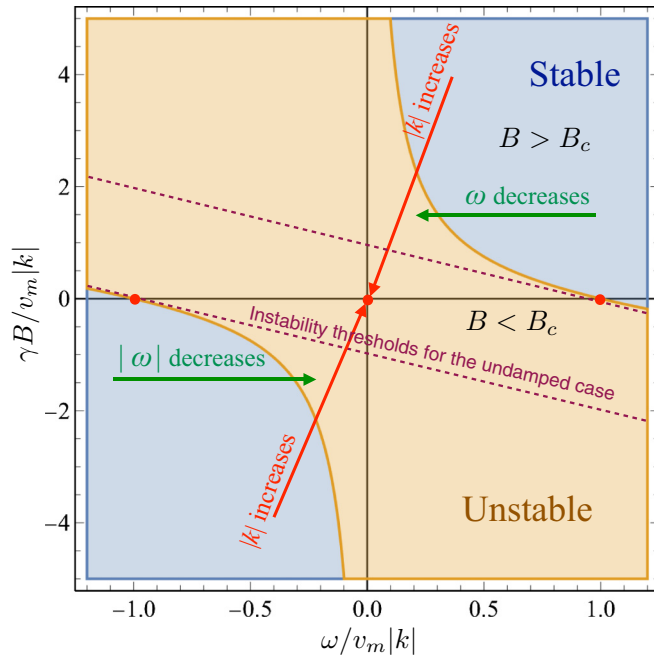


FIG. 2. Stability diagram and critical threshold for the spin superfluid state Eq. (13) parametrized by the normalized Larmor (magnetic field) and precessional ( $\omega$ ) frequencies. The phase-coherent precessional state is stable for magnetic fields above the critical one (blue regions). Red dots indicate the three special points of the diagram, namely,  $(0,0)$  (unstable) and  $(0, \pm 1)$  (stable). Red and green lines display the paths within the diagram parametrized by the increase of the wave vector  $|k|$  (for constant  $B$  and  $\omega$ ) and the decrease of  $|\omega|$  (for fixed  $B$  and  $|k|$ ), respectively. The dashed lines  $|\gamma B + \omega| = v_m |k|$  delineate the boundary of the (expanded) stability region in the absence of damping,  $1/T = 0$ .

This instability condition holds up to the frequencies  $\omega_c = \pm v_m |k|$  along the  $B = 0$  axis. Figure 2 depicts the stability diagram of the spin superfluid state Eq. (13) in terms of the precessional frequency and the external magnetic field. We note that the lines  $\omega = \pm v_m |k|$  delineate the multiparticle continuum of the linearly dispersing excitations (which correspond to the lower frequencies). In the absence of damping,  $1/T = 0$ , the stable region expands to  $v_m |k| < |\gamma B + \omega|$ , which is consistent with the rotating-frame perspective.

## V. DISCUSSION

From Eq. (13), we can clearly extract two length scales for the spin-superfluid phase, namely,  $\ell_p = 2\pi/|k|$  and  $\ell_{nl} = \sqrt{A/\alpha s \omega}$ . The former determines the pitch of the magnetic spiral sustaining the spin-carrying state, whereas the latter determines the spatial rate of change of the associated wave number (due to damping). Our constant-pitch treatment for the instability, based on the local wave number  $k$ , should work when  $k$  does not vary much on the length scale set by fluctuation wavelengths  $q^{-1}$ . This translates into the condition  $\ell_{nl}^{-1} \ll \sqrt{kq}$ . It thus needs to be verified, for internal consistency, that the corresponding lower bound for  $q$  (which becomes progressively smaller as  $\alpha \rightarrow 0$ ) does not significantly affect

the critical magnetic field. Let us now discuss in some detail the physics encapsulated in the corresponding local-stability diagram, Fig. 2.

First, there are three special points in Fig. 2, namely,  $\mathbf{p}_u = (0, 0)$  and  $\mathbf{p}_s^\pm = (0, \pm 1)$ . The former is always unstable, where phase slips are triggered by flapping out of the basal plane. On the other hand,  $\mathbf{p}_s^\pm$  are stable, since here the phase velocity associated with the spin superflow becomes faster than the spin waves and the superfluid cannot relax toward the uniform magnetic configuration. Furthermore, for frequencies beyond the stable critical points, the winding dynamics is stable even in the absence of an applied field. Here, the spin-wave relaxation channels are blocked spectrally (in close analogy to how zeroth sound is spectrally protected against Landau damping in Fermi liquids), even despite the presence of Gilbert damping. This is perhaps the most direct illustration of a dynamical stabilization of winding. Second, keeping  $\omega$  and  $B$  fixed, by increasing the wave vector  $|k|$  we move along the straight path (red lines) that converges asymptotically toward  $\mathbf{p}_u$ , leading to a stability-instability transition. This means, in particular, that when we have a single spin-current injector (e.g.,  $\mu_L \neq 0$  and  $\mu_R = 0$  in the Fig. 1 setup), the local wave vector  $k(x)$  increases toward the injector, where the instability thus sets in first. Third, by fixing  $B$  and  $|k|$  and decreasing the frequency ( $|\omega| \rightarrow 0$ ), we move along the horizontal green lines toward the unstable regime. This case is relevant, for example, when we increase the channel length  $L$  and/or Gilbert damping  $\alpha$ , which would reduce the frequency, according to Eq. (15).

A question that naturally arises is what happens beyond the stability regime. Since the onset of instability occurs close to the injector, we speculate that special boundary solutions (such as the contact-soliton ones found in conventional ferromagnetic platforms [24,25]) or chaotic dynamics may emerge near the injector, which would suppress the overall spin-current injection. A lower but finite spin current may then still propagate in the interior, once the stable regime is reached at a low enough wave vector. We leave it as an open question to elucidate how the unstable boundary dynamics settle into a stable steady flow in the bulk. Finally, as discussed in Ref. [17], the phase-coherent precessional motion between the metallic terminals maps onto a geodesic loop in the order-parameter manifold  $SO(3)$ , so persistent supercurrent states are those associated with the nontrivial class of the fundamental group  $\pi_1(SO(3)) = \mathbb{Z}_2$ : the topological invariant  $\Delta\Phi = 2\pi\nu$  (i.e., the rotation angle between terminals) labels the phase-coherent spin dynamics, with  $\nu$  being the winding number. Spin-carrying states with even  $\nu$  always relax into the ground (current-free) state, and are therefore trivial for spin transport purposes. The degradation of the spin superflow in the absence of magnetic field and for low frequencies occurs via phase slippage mediated by (Anderson-Toulouse)  $4\pi$  vortices [26]. Phase-coherent precessional states with odd  $\nu$  are, however, topologically nontrivial and a mesoscopic residual spin current may prevail,  $\propto |\vec{\nabla}\phi_s| \simeq 2\pi/L$ , which becomes negligible in macroscopic samples. A large enough magnetic field and/or driven frequency precludes the nucleation of these phase-slipping topological textures by hybridizing the out-of-plane rotations.

## ACKNOWLEDGMENTS

This research was supported in part by the National Science Foundation under Grant No. NSF PHY-1748958. R.Z. and J.S. acknowledge support by the Transregional Collaborative Research Center (SFB/TRR) 173 SPIN + X, the Dynamics and Topology Centre funded by the State of Rhineland Palatinate and the Alexander von Humboldt Foundation. Y.T. is supported by the NSF under Grant No. DMR-1742928 and the Alexander von Humboldt Foundation and is grateful for the hospitality of the University of Mainz, where most of this work has been carried out.

## APPENDIX A

The derivation of Eq. (4) utilizes the following intermediate mathematical expressions:

$$\mathbf{q}^* \wedge \partial_\mu (\partial_\mu \mathbf{q} \wedge \mathbf{q}^*) = -\partial_\mu^2 \mathbf{q}^* - (\partial_\mu \mathbf{q} \wedge \partial_\mu \mathbf{q}^*) \mathbf{q}^*, \quad (\text{A1})$$

$$\mathbf{q}^* \wedge (\partial_\mu \mathbf{q} \wedge \mathbf{q}^*) = -\partial_\mu \mathbf{q}^*, \quad (\text{A2})$$

$$\mathbf{q}^* \wedge [(\partial_\mu \mathbf{q} \wedge \mathbf{q}^*) \times \mathbf{B}] = -\partial_\mu \mathbf{q}^* \wedge \mathbf{B} + \frac{1}{2}(\boldsymbol{\omega} \cdot \mathbf{B}) \mathbf{q}^*. \quad (\text{A3})$$

## APPENDIX B

The identities  $\partial_\mu \mathbf{q}_s = \frac{1}{2}(\partial_\mu \phi_s) \boldsymbol{\xi}_3$  and  $\partial_\mu \boldsymbol{\xi}_3 = -\frac{1}{2}(\partial_\mu \phi_s) \mathbf{q}_s$  are straightforward for the unit-norm quaternion parametrizing the spin superfluid state. Therefore, the expressions  $\partial_\mu^2 \mathbf{q}_s = \frac{1}{2}(\partial_\mu^2 \phi_s) \boldsymbol{\xi}_3 - \frac{1}{4}(\partial_\mu \phi_s)^2 \mathbf{q}_s$  and  $\boldsymbol{\omega} = (\partial_t \phi_s) \mathbf{n}$  hold,

which leads to the identities

$$(\partial_t^2 - v_m^2 \vec{\nabla}^2) \mathbf{q}_s = \frac{1}{2}(\partial_t^2 \phi_s - v_m^2 \partial_x^2 \phi_s) \boldsymbol{\xi}_3 - \frac{1}{4}[(\partial_t \phi_s)^2 - v_m^2 (\partial_x \phi_s)^2] \mathbf{q}_s, \quad (\text{B1})$$

$$\lambda(\mathbf{q}_s) = \frac{1}{4}[(\partial_t \phi_s)^2 - v_m^2 (\partial_x \phi_s)^2] + \frac{\gamma}{2} B \partial_t \phi_s, \quad (\text{B2})$$

$$\mathbf{B}^* \wedge \partial_t \mathbf{q} = \frac{1}{2}(B \partial_t \phi_s) \mathbf{q}_s, \quad (\text{B3})$$

$$\partial_t \mathbf{B}^* \wedge \mathbf{q} = -(\partial_t B) \boldsymbol{\xi}_3. \quad (\text{B4})$$

As a result, Eq. (4) becomes

$$\left[ \partial_t^2 \phi_s + \frac{1}{T} \partial_t \phi_s - v_m^2 \partial_x^2 \phi_s + \gamma \partial_t B \right] \boldsymbol{\xi}_3 = \mathbf{0}, \quad (\text{B5})$$

which, in turn, leads to Eq. (5) since  $\boldsymbol{\xi}_3 \neq \mathbf{0}$ .

Furthermore, for the lateral configuration depicted in Fig. 1, we have  $\hat{n}_L = -\hat{n}_R = \hat{x}$ . With account of the parametrization  $w = \cos(\phi/2)$ ,  $\mathbf{v} = \sin(\phi/2) \mathbf{n}$  for the order parameter, Eqs. (9) and (10) become

$$\mathcal{A} \partial_x \phi \left( -\frac{L}{2}, t \right) = \frac{gL}{4\pi} \left[ -\mu_L + \hbar \partial_t \phi \left( -\frac{L}{2}, t \right) \right], \quad (\text{B6})$$

$$\mathcal{A} \partial_x \phi \left( \frac{L}{2}, t \right) = \frac{gR}{4\pi} \left[ \mu_R - \hbar \partial_t \phi \left( \frac{L}{2}, t \right) \right]. \quad (\text{B7})$$

By introducing next the phase-coherent precessional ansatz  $\phi_s$  into them, which satisfies  $\partial_x \phi_s = k + \mu x/v_m^2$  and  $\partial_t \phi_s = \mu T$  under a static magnetic field, Eqs. (11) and (12) are straightforwardly derived.

## APPENDIX C

Equations (17) and (18) are derived by incorporating the parametrization Eq. (16) into Eq. (4) and expanding up to first order in the fluctuation fields. The following intermediate results have been used:

$$\partial_\mu^2 \mathbf{q} \simeq -\left[ \frac{1}{4}(\partial_\mu \phi_s)^2 + \partial_\mu \Psi_l \partial_\mu \phi_s + \frac{1}{2} \Psi_l \partial_\mu^2 \phi_s \right] \mathbf{q}_s + \hat{e}_+ \partial_\mu^2 \Psi_t + \hat{e}_- \partial_\mu^2 \Psi_t^* + \left[ \partial_\mu^2 \Psi_l + \frac{1}{2} \partial_\mu^2 \phi_s - \frac{1}{4} \Psi_l (\partial_\mu \phi_s)^2 \right] \boldsymbol{\xi}_3, \quad (\text{C1})$$

$$\partial_\mu \mathbf{q} \simeq -\frac{1}{2} \Psi_l \partial_\mu \phi_s \mathbf{q}_s + \hat{e}_+ \partial_\mu \Psi_t + \hat{e}_- \partial_\mu \Psi_t^* + \left[ \partial_\mu \Psi_l + \frac{1}{2} \partial_\mu \phi_s \right] \boldsymbol{\xi}_3, \quad (\text{C2})$$

$$\lambda(\mathbf{q}) \simeq \left[ \frac{1}{4}(\partial_t \phi_s)^2 - \frac{1}{4} v_m^2 (\vec{\nabla} \phi_s)^2 + \frac{\gamma}{2} \partial_t \phi_s B \right] + \left[ \partial_t \Psi_l \partial_t \phi_s - v_m^2 \vec{\nabla} \Psi_l \cdot \vec{\nabla} \phi_s + \gamma \partial_t \Psi_l B \right], \quad (\text{C3})$$

$$\mathbf{B}^* \wedge \partial_t \mathbf{q} \simeq -\frac{1}{2} (\Psi_l \partial_t \phi_s) \mathbf{B}^* \wedge \mathbf{q}_s + \partial_t \Psi_l \mathbf{B}^* \wedge \hat{e}_+ + \partial_t \Psi_t^* \mathbf{B}^* \wedge \hat{e}_- + (\partial_t \Psi_l + \frac{1}{2} \partial_t \phi_s) \mathbf{B}^* \wedge \boldsymbol{\xi}_3, \quad (\text{C4})$$

$$\partial_t \mathbf{B}^* \wedge \mathbf{q} \simeq \partial_t \mathbf{B}^* \wedge \mathbf{q}_s + \Psi_t \partial_t \mathbf{B}^* \wedge \hat{e}_+ + \Psi_t^* \partial_t \mathbf{B}^* \wedge \hat{e}_- + \Psi_l \partial_t \mathbf{B}^* \wedge \boldsymbol{\xi}_3, \quad (\text{C5})$$

$$\mathbf{B}^* \wedge \mathbf{q}_s = -B \boldsymbol{\xi}_3, \quad \mathbf{B}^* \wedge \boldsymbol{\xi}_3 = B \mathbf{q}_s, \quad \mathbf{B}^* \wedge \hat{e}_\pm = \pm i B \hat{e}_\pm. \quad (\text{C6})$$

- 
- [1] P. Upadhyaya, S. K. Kim, and Y. Tserkovnyak, *Phys. Rev. Lett.* **118**, 097201 (2017).  
[2] Y. Tserkovnyak and M. Kläui, *Phys. Rev. Lett.* **119**, 187705 (2017).  
[3] E. B. Sonin, *Solid. State Commun.* **25**, 253 (1978).  
[4] E. B. Sonin, *Zh. Eksp. Teor. Fiz.* **74**, 2097 (1978) [*JETP* **47**, 1091 (1978)].  
[5] E. B. Sonin, *Pis'ma Zh. Eksp. Teor. Fiz.* **30**, 697 (1979) [*JETP Lett.* **30**, 662 (1980)].  
[6] J. König, M. C. Bø nsager, and A. H. MacDonald, *Phys. Rev. Lett.* **87**, 187202 (2001).  
[7] E. B. Sonin, *Adv. Phys.* **59**, 181 (2010).  
[8] S. Takei and Y. Tserkovnyak, *Phys. Rev. Lett.* **112**, 227201 (2014).  
[9] S. Takei, B. I. Halperin, A. Yacoby, and Y. Tserkovnyak, *Phys. Rev. B* **90**, 094408 (2014).  
[10] W. Chen and M. Sigrist, *Phys. Rev. Lett.* **114**, 157203 (2015).

- [11] W. Yuan, Q. Zhu, T. Su, Y. Yao, W. Xing, Y. Chen, Y. Ma, X. Lin, J. Shi, R. Shindou, X. C. Xie, and W. Han, *Sci. Adv.* **4**, eaat1098 (2018).
- [12] P. Stepanov, S. Che, D. Shcherbakov, J. Yang, K. Thilahaar, G. Voigt, M. W. Bockrath, D. Smirnov, K. Watanabe, T. Taniguchi, R. K. Lake, Y. Barlas, and A. H. MacDonald, and C. N. Lau. *Nat. Phys.* **14**, 907 (2018).
- [13] T. Dombre and N. Read, *Phys. Rev. B* **39**, 6797 (1989).
- [14] P. Azaria, B. Delamotte, and D. Mouhanna, *Phys. Rev. Lett.* **68**, 1762 (1992).
- [15] A. V. Chubukov, T. Senthil, and S. Sachdev, *Phys. Rev. Lett.* **72**, 2089 (1994).
- [16] Y. Tserkovnyak and H. Ochoa, *Phys. Rev. B* **96**, 100402(R) (2017).
- [17] H. Ochoa, R. Zarzuela, and Y. Tserkovnyak, *Phys. Rev. B* **98**, 054424 (2018).
- [18] B. I. Halperin and W. M. Saslow, *Phys. Rev. B* **16**, 2154 (1977).
- [19] J. Sinova, S. O. Valenzuela, J. Wunderlich, C. H. Back, and T. Jungwirth, *Rev. Mod. Phys.* **87**, 1213 (2015).
- [20] The concept of spin mixing conductance [21] admits a microscopic definition for glassy systems in the regime of weak spin-orbit coupling [16,22]. In this paper, we introduce the spin-mixing conductance as a phenomenological parameter that would ultimately relate the torque to the driven electrical current (in conjunction with the spin Hall phenomenology) [23], regardless of the strength of the spin-orbit interaction.
- [21] Y. Tserkovnyak, A. Brataas, G. E. W. Bauer, and B. I. Halperin, *Rev. Mod. Phys.* **77**, 1375 (2005).
- [22] M. F. Jakobsen, A. Qaiumzadeh, and A. Brataas, *Phys. Rev. B* **100**, 134431 (2019).
- [23] Y. Tserkovnyak and S. A. Bender, *Phys. Rev. B* **90**, 014428 (2014).
- [24] E. Iacocca and M. A. Hofer, *Phys. Rev. B* **99**, 184402 (2019).
- [25] T. Schneider, D. Hill, A. Kakay, K. Lenz, J. Lindner, J. Fassbender, P. Upadhyaya, Y. Liu, K. Wang, Y. Tserkovnyak, I. N. Krivorotov, and I. Barsukov, *Phys. Rev. B* **103**, 144412 (2021).
- [26] P. W. Anderson and G. Toulouse, *Phys. Rev. Lett.* **38**, 508 (1976).